Hindawi
International Transactions on Electrical Energy Systems
Volume 2023, Article ID 2073742, 14 pages
https://doi.org/10.1155/2023/2073742

Research Article

PV Based Standalone DC -Micro Grid System for EV Charging Station with New GWO-ANFIS MPPTs under Partial Shading Conditions

R. Ragul,[1] N. Shanmugasundaram,[1] Mariaraja Paramasivam,[2] Suresh Seetharaman,[3] and Sheela L. Mary Immaculate[4]

[1]*Department of Electrical and Electronics Engineering, Vels Institute of Science, Technology & Advanced Studies (VISTAS), Chennai, Tamil Nadu, India*
[2]*Department of Electrical and Electronics Engineering, P. A. College of Engineering and Technology, Pollachi, Tamil Nadu, India*
[3]*Department of Electrical and Electronics Engineering, Kalaignar Karunanidhi Institute of Techonology (KIT), Coimbatore, Tamil Nadu, India*
[4]*DEAN-PESAC, Pentecost University, Accra, Ghana*

Correspondence should be addressed to Sheela L. Mary Immaculate; misheela@pentvars.edu.gh

Received 18 August 2022; Revised 11 October 2022; Accepted 24 November 2022; Published 15 March 2023

Academic Editor: Ravi Samikannu

The goal of this article is to use MPPTs (maximum power point trackers) to extort maximum power from best configuration or combine renewable resources and energy storage systems that all work together in off-grid for electric vehicle charging. The grey wolf algorithm (GWO) searches the MPP at partial shading condition (PSC) with following two consideration one is high oscillations around GMPPs, and other is that they are unable to track the new GMPPs after it has changed positions because the seeking agents will be busy around the previous GMPPs captured. Hence, in this paper, the proposed research objective is to find solutions to these two difficulties. The issue of oscillations around GMPPs was handled by combining GWO with ANFISs (adaptive Neuro-Fuzzy inference system) to gently tune output produced power at GMPPs. ANFISs are distinguished by their near-zero oscillations and precise GMPPs capturing. The second issue called they are unable to track the new GMPPs after it has changed positions is addressed in this work by using novel initialization by GWOs (Grey wolf Optimizations). In the MATLAB-Simulink and experiments demonstrate the effectiveness of the suggested GWO-ANFIS MPPTs based off-grid station for EVs (Electrical Vehicle) battery charging.

1. Introduction

With the growing environmental concerns, governments throughout the world have established a variety of carbon emission limits. EVs that are powered entirely by electricity have the potential to replace gasoline and diesel vehicles. EVs enhance energy efficiency through effective fuel economy, especially when the power is generated from renewable sources such as solar and wind. When it comes to EVs in smart grids, that are more than simply an electrical burden, but also a power resource [1, 2], several proposals have been made [3–7] presented an approach for modelling EVs as an additional load on the distribution network. Several scholars [8, 9] proposed a grid-connected PV system for EVs charging. In most cases, a backup battery is not required for a grid-connected system. There are two configurations for the grid-connected system. One is that the PV system works in conjunction with the utility grid to provide electricity to the load. As a result, the output of PV system is frequently less than load's power. The other is that the PV system is designed to provide the load with the needed power, and the utility grid serves as a backup source during solar power variations in this arrangement. With the ever-increasing

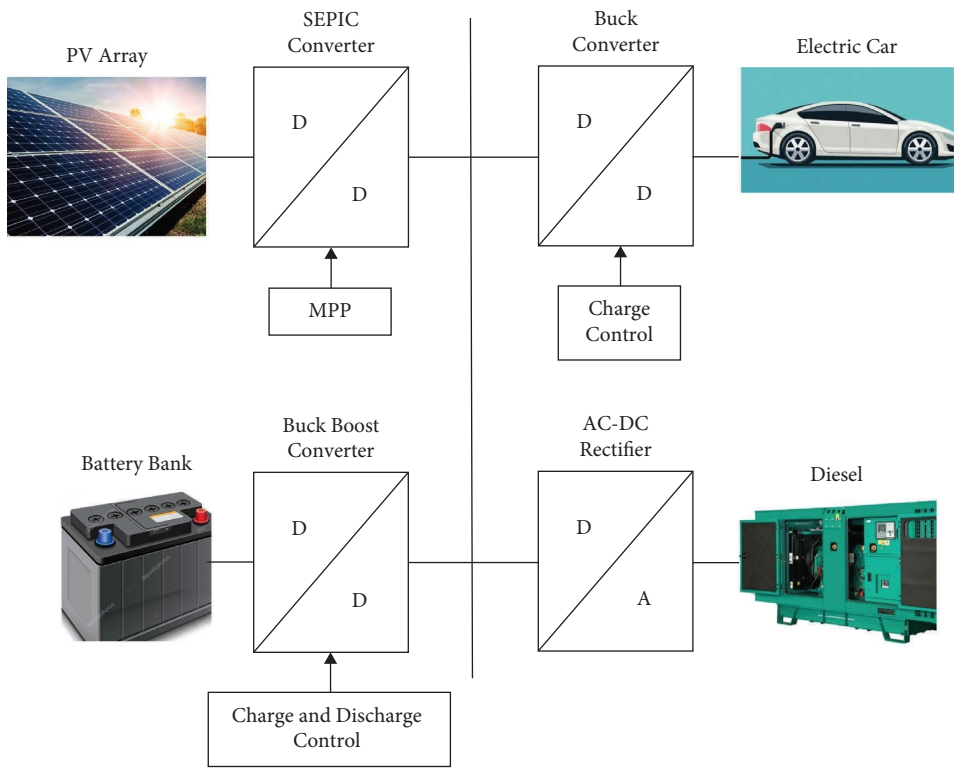

Figure 1: Off-grid charging station for EVs.

demand for electric vehicles, it became imperative to expand the number of charging stations. EVs require a high number of charging stations. As a result, EVs will be a substantial burden on the future distribution network system. The phrase "off-grid" of PV systems are not linked to main grids is known as a "stand-alone" PV systems. These stand-alone PV systems are ideal for electrifying small places in remote areas or small towns. They can also be used as charging points for EVs on long-distance routes as depicted in Figure 1. Many publications [10, 11] have discussed off-grid system design.

Due to seasonal weather conditions and the non-linear nature of solar irradiation, solar power output varies significantly, necessitating a hybrid application or backup systems [12]. Solar irradiance is not strongly connected across surrounding locations over short time periods, which is a critical factor in PV power output losses and swings [13]. MPPTs are considered significant components of PV systems for increased efficiency. Because of the non-linear features of PV arrays, it is unavoidable to design an effective maximum power point tracking system which is not only effective and improves the solar power system's output power [14]. Furthermore, a variety of internal and external factors including series/parallel resistances, Diode factors, solar irradiations, PV array surfaces, internal temperatures, shadows and dirt impact on PV system's output efficiencies. Because the dynamics of PV systems under PSCs change over time, MPPTs for PV powered systems must track GMPPs smoothly and steadily in a variety of situations including shades, degraded PVs, changes in PV arrays or PV characteristics.

A number of algorithms for MPPTs have been suggested for enhancing PV system's effectiveness, including hill climbing [12], P&O (perturb and observe) [15–17], incremental conductance [18], however these techniques produce oscillations at MPPTs, resulting in power losses. IC technique [18] was developed to decrease these oscillations and increase module efficiency, however it only lowered the oscillations. P&O and IC approaches failed in time spans specified by changing atmospheric conditions. A scanning technique was presented [19–21] to estimate panel's maximum power-delivering potential at any given operational condition for PV systems with rapidly changing and PSCs and insolations.

Soft computing methods employed for MPPTs in PV systems include PSOs (Particle Swarm Optimizations) [22], GWOs [23], CS, ACOs (Ant Colony Optimizations) [24], KHOs (Krill Herd Optimizations), FAs (Firefly algorithms) [25], ABCs (artificial bee colonies), MVOs (Multi-Verse Optimizations), ALOs (Ant Lion Optimizations), SCAs (Sine Cosine Algorithms), Dragonfly Algorithms, WOAs (Whale Optimization Algorithms), MFOs (Moth-Flame Optimizations). Several studies [26, 27] have examined and introduced all of these approaches. In shaded or non-shaded circumstances where most approaches could catch the GMPPs. Nonetheless, they are affected by two major issues in PV applications. The first difficulty is with dynamic or time-varying GMPPs location in P-V curves, where most of these techniques may catch the initial GMPPs and stay around it, but not if the GMPP positions changes over a period of time. The second difficulty is that random variables associated with all of these soft computing techniques create substantial power swings near steady states. To overcome these two challenges, novel and efficient ways have been applied in this

study where the first issue is overcome by introducing re-initialization methods for soft computing methodologies while the second issue is resolved by using combination of soft computing techniques namely GWOs and ANFISs and where quick peak tracking and low oscillations around GMPPs differentiate ANFISs.

2. Related Work

Controller settings were optimised and adaptively modified using a predictive neural networks controller by Mohamed et al. [28]. The scheme anticipated control parameters by tracking grid current and dc-bus voltage mean square errors and eliminating them in a specified amount of time.

SMCs were proposed by Pahari and Subudhi [29] for control discontinuity based on high frequency conversions for driving closed loop systems to reach and stay on planned sliding surfaces. This approach considerably enhanced PV system's tracking speeds, however the step size of modulation depths of switching devices impacted system's dynamic and steady-state properties. When ΔU increased, Although tracking speeds increased, variations in PV array's output powers and voltages also increased. Pahari and Subudhi introduced Integral sliding mode controls to increase controller's steady state performances.

External voltage control, P&O, and an adaptive integral differential slip films were used to design their new sliding surface in Kihal et al. [30] and where derivative and integral terms eliminated overshoots during quick solar irradiation changes and reduced steady-state fluctuations.

The study in [31] was a novel model of adaptive PID controllers based on ANFISs proposed to address concerns in MPPTs approaches. It aided in maximising the output of DC pump in terms of speed. Their proposed controller was also used to test performances of EVs. To get the maximum power from solar-powered pump many methods have been tried and ANFISs have also been used to optimise performances of these intelligent systems. However, the approaches have certain flaws, necessitating the development of a new paradigm. As a result, in this research, a technique is developed in which a PID controller is used, and the combination of ANFISs and PID improves the performance of MPPTs. Moreover, this work's proposed combinations were tested on EVs.

Padmanaban et al. [32] presented grid-based PV systems with MPPT control mechanisms. Their work's ABC method converted ANFIS membership functions and their experimental study demonstrated that PV grid integrations were dependable and safe.

The author of [33] recommended modifying INC (Incremental Conductance) to track GMPPs of PV systems with PSCs without the application of any nature-inspired intelligence approaches like PSOs or other comparable algorithms. The work identified p-v curve as a mixture of areas and monitored global peaks by moving operating points from one region to another. In addition, the system incorporated varying sample times for quicker global peak tracking under extreme PSCs caused by unpredictable PV module shading patterns. Their PV module was modelled in combination with SEPIC converters for a battery charging applications using MATLAB/SIMULINK platform. The proposed technique was put to the test under various shading patterns to see how quickly and accurately their tracker tracked the power points. Finally, the suggested algorithm's idea was tested using PILs (Process-in-Loops) on TMS320F28027 LAUNCHPAD DSP board. Their result comparisons with recently published work in this sector showed that their suggested approach was more beneficial in terms of processing times.

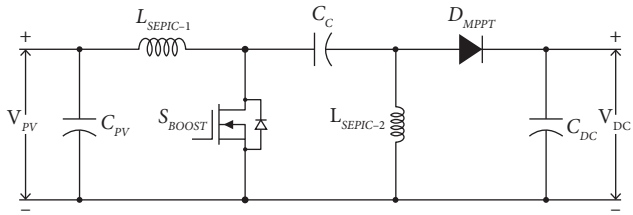

Figure 2: The SEPIC converter diagram.

Hence Evolutionary algorithms have reduced steady state oscillations and have advantage of ease in implementation and simplicity of computation.

3. Design Charging Station Converters

The power converter is the most important technology associated with PV systems. Maximum power from PV module is dragged from converter and sent to the load. This should be accomplished in grid-connected systems with least harmonic content in the current and a PF value greater than 0.9. The output voltage in off-grid systems should be adjusted to the necessary value. The suggested charging station in Figure 1 employs three DC-DC converter topologies. The SEPIC converter converts the fluctuating voltage from modules to a stable voltage, while the buck converter reduces the DC Bus voltage to voltage of the electric vehicle battery. The bidirectional converter is use d to control the battery bank's charging and discharging. The following sections detail the design of three DC-DC converters.

3.1. DC-DC SEPIC Converter. Figure 2 depicts Single Ended Primary Inductance Converter. [34] contains PV modules' input source voltage (V_{PV}), SEPIC inductor ($L_{SEPIC-1}$ and $L_{SEPIC-2}$), Coupling Capacitor (C_C), DC-link capacitor (C_{DC}), a diode (D_{MPPT}), MOSFET (Metal–Oxide–Semiconductor Field- Effect Transistor) (S_{MPPT}) as a switch and the output voltage (V_{DC}) (DC Bus Voltage). The SEPIC converter's output voltage can reduce or enhance the input PV voltage. Controlling or changing voltage may be done by adjusting the MOSFET's duty cycle.

As per the equation (34), the output voltage V_{DC} is proportionate to input voltage V_{PV}.

$$D_{MPPT} = \frac{V_{DC}}{V_{PV} + V_{DC}}, \tag{1}$$

here D_{MPPT} is duty cycle.

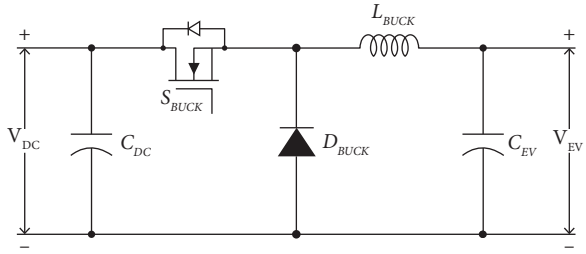

Figure 3: The buck converter diagram.

Equation (1) is use d to determine duty cycle of SEPIC converter. Solar energy ranges between 0 and 1000 W/m^2 and temperature ranges from 25 to 75 degrees Celsius in the simulation.

SEPIC converter duty cycle is determined for a cell temperature of 25°C and irradiance of 1000 W/m^2 in non-shaded conditions. $V_{\mathrm{PV}} = 116$ V, as you may have observed. When V_{DC} is equal to 110 V, $D_{MPPT\,(\mathrm{MIN})}$ at 110 V is 0.48.

If the two PV panels are shaded, the SEPIC Converter Duty Cycle is calculated at 25°C and 1000 W/m^2 at cell temperature of 25°C. As observed, $V_{\mathrm{PVmin}} = 58$ V and $V_{\mathrm{DC}} = 110$ V, resulting in $D_{\mathrm{MPPT\,(Max)}}$ at 110 V of 0.65. Then inductance for continuous current, Coupling Capacitor of SEPIC converter is calculated below

3.1.1. Design of SEPIC Inductor. In the SEPIC converter, the inductance for continuous current is computed as follows [34]:

$$\begin{aligned} L_{SEPIC-1}\&L_{SEPIC-2} &= \frac{V_{\mathrm{PVmin}}\left(D_{MPPT\,(Max)}\right)}{\Delta I_{o\,\mathrm{Max}} * F_{SW}} \\ &= 1.58\,mH \cong 1.6mH. \end{aligned} \tag{2}$$

The switching frequency, F_{SW}, has been set at 25 kHz. The ripple current $\Delta I_{o\,\mathrm{Max}}$ is computed as follows: VIN is the converter input voltage = 58 V. (taken as 13 percent of the total current):

$$\begin{aligned} \Delta I_{LBoost} &= 0.13 * I_{PV} \\ &= 0.13 * 7.34 \\ &= 0.95. \end{aligned} \tag{3}$$

3.1.2. Design of SEPIC Coupling Capacitor. Coupling capacitor C_c ripple voltage is:

$$\begin{aligned} C_C &= \frac{I_{PV}\left(1 - D_{MPPT\,(Max)}\right)}{\Delta V_{CC} * F_{SW}} \\ &= \frac{7.35\,(1 - 0.65)}{12 * 25} \\ &= 8.5uF \cong 10uF. \end{aligned} \tag{4}$$

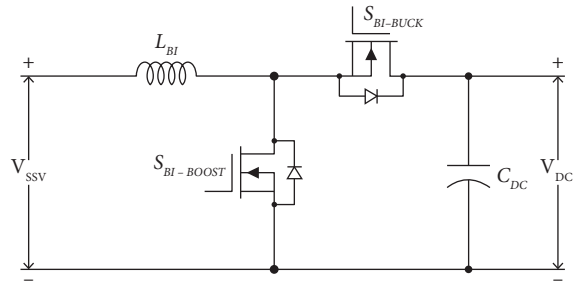

Figure 4: The bidirectional converter diagram.

3.2. DC-DC Buck Converter. Buck converter illustrated in Figure 3 [35] is made up of DC-link voltage as an input source (V_{DC}), buck inductor (L_{BUCK}), buck capacitor (C_{BUCK}), a diode (D), MOSFET (S) as a switch and the output voltage (V_{EV}) as an EVs battery voltage (350 V in Tesla S 100D cars).

The duty ratio is calculated as follows:

$$\begin{aligned} D_{BUCK} &= \frac{V_{EV}}{V_{DC}} \\ &= \frac{60}{110} \\ &= 0.545. \end{aligned} \tag{5}$$

3.2.1. Design of Buck Inductor and Buck Capacitor. The buck converter's inductance for continuous current is computed as follows [35]:

$$\begin{aligned} L_{BUCK} &= \frac{V_{DC} - V_{EV}}{\Delta I_{LBUCK} * F_{SW}} \\ &= \frac{110 - 60}{1.51 * 10,000} \\ &= 3.3\,mH, \end{aligned} \tag{6}$$

ΔI_{LBUCK} (The ripple current) is computed as (taken as 13% of the charge current):

$$\begin{aligned} \Delta I_{LBUCK} &= 0.13 * I_{CGB} \\ &= 0.013 * 11.66 \\ &= 1.51A. \end{aligned} \tag{7}$$

3.3. The Bidirectional Converter. The storage battery is supplied as a backup service during energy outages to smooth power storage produced by off-grid systems. As a consequence of the advantages listed below, this article recommends a bidirectional buck-boost converter, as illustrated in Figure 4 [23], regulate storage and delivery of electricity among PV system and battery bank:

(i) It provides the most cost-effective solution with the fewest external components.

(ii) It accomplishes voltage step-up and step-down using the fewest possible components.

(iii) It has a decreased duty cycle when in operation.

(iv) It has a high efficiency over a wide range of input and output voltages.

(v) It is less costly than the majority of converters.

Based on power flow direction, the bidirectional converter may be configured in two operation modes: boost and buck [36] describes these modalities in detail.

3.3.1. Design for the Bidirectional Converter. The inductance (L BI) can be represented in two different ways:

In Buck mode:

$$\begin{aligned} L_{BI-Buck} &= \frac{V_{DC} - V_{SSV}}{\Delta I_{BI-BUCK} * F_{SW}} \\ &= \frac{110 - 60}{2.08 * 10,000} \\ &= 2.4\,mH, \end{aligned} \tag{8}$$

$\Delta I_{BI-\text{Buck}}$ (ripple current) is computed as (taken as 13% of charge current):

$$\begin{aligned} \Delta I_{BI-BUCK} &= 0.13 * I_{CGS} \\ &= 0.13 * 16 \\ &= 2.08A. \end{aligned} \tag{9}$$

In Boost mode:

$$\begin{aligned} L_{BI-BOOST} &= \frac{V_{DC} - V_{SSV}}{\Delta I_{BI-BOOST} * F_{SW} * V_{DC}} \\ &= \frac{110 - 60}{1.65 * 10,000 * 110} \\ &= 0.02mH, \end{aligned} \tag{10}$$

here ΔI_{BI} (ripple current) under Boost mode is computed as (taken as 13% of the charge current):

$$\begin{aligned} \Delta I_{BI-BOOST} &= 0.13 * I_{CGS}\,\frac{V_{DC}}{V_{SSV}} \\ &= 0.13 * 6.95 * \frac{110}{60} \\ &= 1.65\,A, \end{aligned} \tag{11}$$

$L_{BI-\text{Buck}}$ is more than $L_{BI-BOOST}$ to make sure that inductor current can function during continuous conduction mode (CCM) [36], $L_{BI-BUCK}$ value is selected, that is, equal to 2.4 mH here $D_{BI-\text{BOOST}}$ is duty cycle under Boost mode and computed as:

$$\begin{aligned} D_{BI-BOOST} &= 1 - \frac{V_{SSV}}{V_{DC}} \\ &= 1 - \frac{60}{110} \\ &= 0.455. \end{aligned} \tag{12}$$

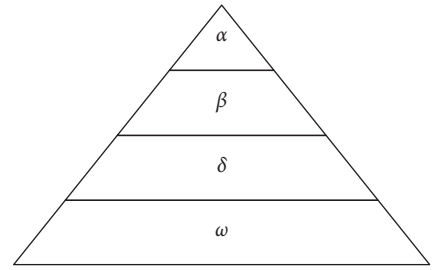

Figure 5: Leadership pyramid with four level (α, β, δ and ω).

4. Design of Closed Loop System

The Grey wolf Optimizer combined with ANFISs are implemented to track the new GMPPs after it has changed positions are discussed follows.

4.1. Proposed Grey Wolf Optimizer Combined with ANFISs Global Maximum Power Point Tracking Techniques. Due the PSC the PV array generates the several peaks is generated with various LMPPs and a single GMPPs so tracking of maximum power location is obtain by GWO algorithm. The GWO enhance power quality and ensure the efficiency of PVCs (photovoltaic cells) under PSCs (partial shading conditions) by varying the duty cycle with low iteration. Mirjalili et al. originally proposed Grey Wolf Optimizer in 2014 [23], and it is considered one of the most recent heuristic optimization techniques. This approach is based on the way grey wolves hunt food in the wild, pursuing, attacking, and killing them. Grey wolves prefer to live in packs of 5 to 10 individuals. They follow a strict social dominance structure with four levels of leadership. Leaders, named as alpha (α), and subleaders, which they call beta (β), etc, are referred to as leadership pyramids, as illustrated in Figure 5, where wolf dominance rises from top to bottom [37]. The alpha wolf holds duty cycle of maximum power by corresponding random search duty cycle set. Accordingly the second and third maximum powers are named as beta and delta respectively. The rest of maximum power solution at the duty cycle is denoted as omega. The tracking global maximum power behaviour of grey wolves, we suppose that the alpha, beta and delta have the better knowledge about the

global maximum power. Therefore, we save the first to three best powers obtained so far iterations and oblige the next iteration search duty cycle to update the duty cycle according to the best maximum power. GWOs are created to replicate grey wolves behaviour in the optimization domain. Grey wolf leadership hierarchy is established by assuming the leaders; wolves known as alpha (α), subleaders known as beta (β), lower rank wolves known as delta (δ), lowest rank wolves known as omega (ω).

Grey wolves encircle food in the hunt, as previously stated. The following equations are presented to analytically model encircling behaviour [23]:

$$\begin{aligned} \overrightarrow{E} &= \left|\overrightarrow{C}.\overrightarrow{D_P}(t) - \overrightarrow{D}(t)\right|, \\ \overrightarrow{D_P}(t+1) &= \overrightarrow{D_P}(t) - \overrightarrow{A}.\overrightarrow{E}, \end{aligned} \tag{13}$$

here t indicates current iteration, A, C are coefficient vectors whose values has capability to save balance between exploration and exploitation in searching region, D_P is prey's position vector, D represents grey wolf's position vector. Two coefficient vectors A and C are computed like:

$$\begin{aligned} \overrightarrow{A} &= 2\overrightarrow{a}.\overrightarrow{r_1} - \overrightarrow{a}, \\ C &= 2.\overrightarrow{r_2}, \end{aligned} \tag{14}$$

here, coefficient a is decreasing linearly beginning 2 to 0, r_1, r_1 are arbitrary vectors with value [1, 0]. Grey wolves hunt by circling their prey, and pack should follow the commands of alpha wolf (D_α) as a high priority, and orders of the beta wolves (D_β) and delta wolves (D_δ) as a lesser priority. The following equations can be used to model this leadership hierarchy numerically:

$$\begin{aligned} \overrightarrow{E_\alpha} &= \left|\overrightarrow{C_1}.\overrightarrow{D_\alpha} - \overrightarrow{D}\right|, \\ \overrightarrow{E_\beta} &= \left|\overrightarrow{C_2}.\overrightarrow{D_\beta} - \overrightarrow{D}\right|, \\ \overrightarrow{E_\delta} &= \left|\overrightarrow{C_3}.\overrightarrow{D_\delta} - \overrightarrow{D}\right|, \\ \overrightarrow{D_1} &= \overrightarrow{D_\alpha} - \overrightarrow{A}_1.\overrightarrow{E_\alpha}, \\ \overrightarrow{D_2} &= \overrightarrow{D_\beta} - \overrightarrow{A}_2.\overrightarrow{E_\beta}, \\ \overrightarrow{D_3} &= \overrightarrow{D_\delta} - \overrightarrow{A}_3.\overrightarrow{E_\delta}, \\ \overrightarrow{D_P}(t+1) &= \frac{\overrightarrow{D_1} + \overrightarrow{D_2} + \overrightarrow{D_3}}{3}. \end{aligned} \tag{15}$$

The solution's exploration and exploitation are determined by a and A *values*, wherein $|A| \le 1$, the wolves incline to exploitation (converge to prey) and $|A| \ge 1$, wolves tend to exploration (diverge from prey as it might be one of LMPPs). As stated in introduction, hybrid GWO-ANFIS is suggested to combine benefits of both approaches and monitor variant GMPPs under variation PSCs with almost negligible oscillations around GMPPs power. To monitor the variation GMPPs, GWOs with two re-initialization approaches is presented. GWOs is re-initialized to seek for GMPPs at first. After GWOs has caught initial GMPPs, it is ended depending on first condition and the role is given to ANFISs [38]. ANFISs are employed to soften the initial GMPPs captured by GWOs and track precise value of GMPPs with nearly minimal fluctuation around global power. Inputs of ANFISs are V_{PV}, I_{PV} and T_{PV} [28], which create the Duty (D_{MPPT}) output, whereas the ANFISs output is the DC-DC converter's optimum duty ratio (SEPIC converter) [39, 40]. In contrast, if the PSCs changes, ANFISs are terminated, and GWOs must be re-initialized to search for and follow new GMPPs, as illustrated in Figure 6.

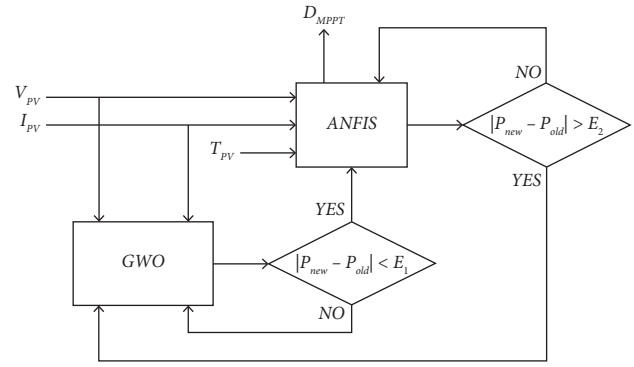

Figure 6: PV energy system with hybrid GWO-ANFIS based MPPTs.

This study proposes a combination of GWOs and ANFISs for taking full advantage of both techniques while overcoming their disadvantages. When it comes to capturing GMPPs of PV systems, GWOs are the most effective and have the fastest convergences, but it also has a lot of oscillations around GMPPs at steady states. ANFISs which are opposite of GWOs remain at local peaks with extremely low oscillations around GMPPs. As a result, GWOs were first used to quickly and effectively track GMPPs and subsequently ANFISs then start to behave like MPPTs with very low oscillations. As a result, GWOs are employed to follow the GMPPs and avoid local peaks at the start of MPPTs. Furthermore, at GMPPs, the drawback of major oscillations is avoided by pausing operations and enabling ANFISs to operate with extremely low oscillations. In order for GWOs to be terminated and ANFISs to complete the control of MPPTs on GMPPs that have already been captured, the following prerequisites must be met:

$$\left|P_{new} - P_{old}\right| \le E_1, \tag{16}$$

here, P_{new} is current power obtained from PV system, P_{old} is pervious iteration value of simulation, E_1 is permissible limit before transferring control from GWOs to ANFISs, that is equivalent to 2% of generated power. Condition for terminating ANFISs and go back to GWOs to re-initialize the agents to search for new GMPPs under new PSCs via following conditions:

$$\left|P_{new} - P_{old}\right| \ge E_2, \tag{17}$$

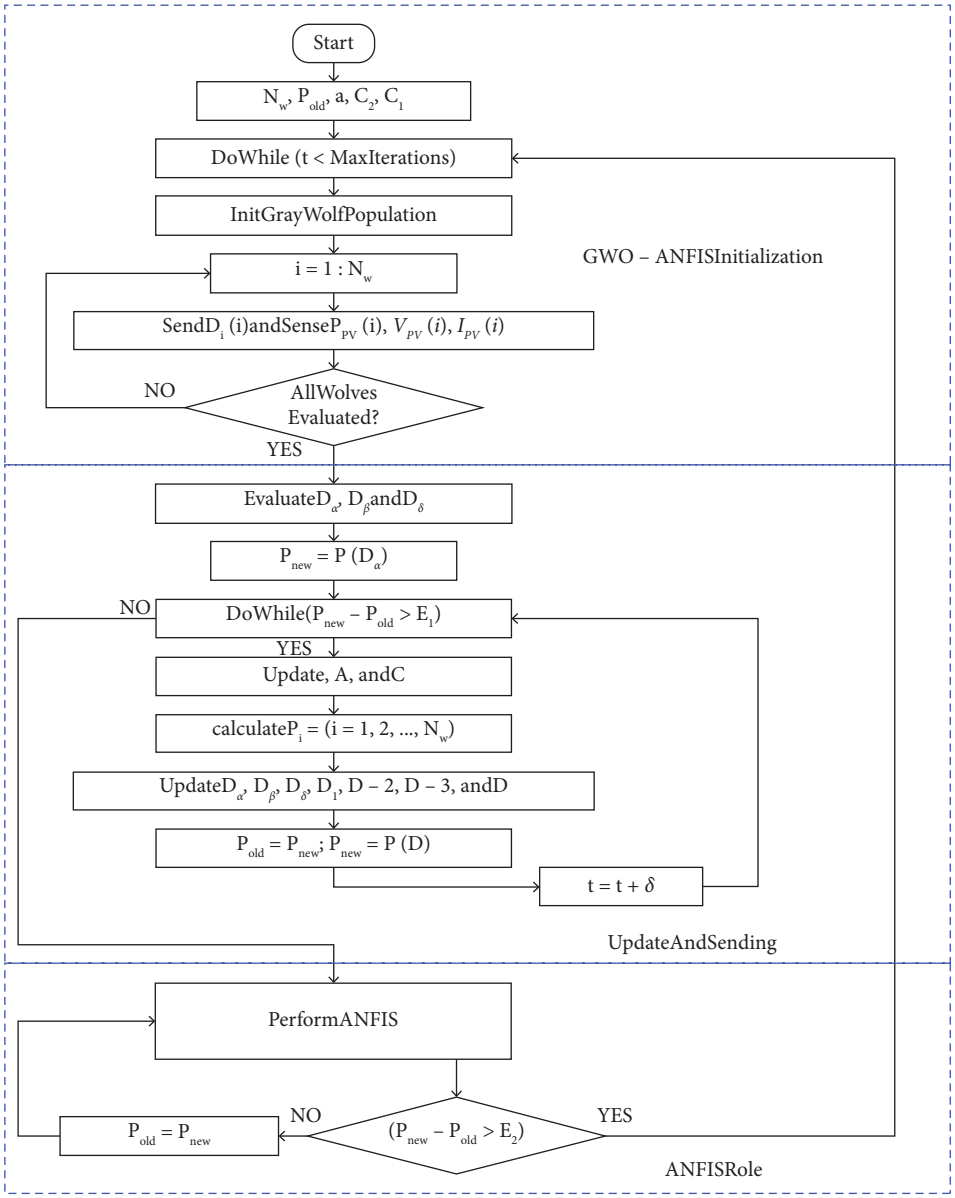

Figure 7: Flowchart of GWO-ANFIS based on PSCs change.

here E_2 is permissible limit before transferring control from ANFISs to GWOs, that equivalent to 5% of generated power.

There are two suggested initialization approaches for re-initializing the GWOs to begin looking for a new GMPPs. As previously stated, the goal of combining GWOs and ANFISs is to take advantages of both approaches, with GWOs being rapid and reliable MPPTs approach for tracking GMPPs under PSCs while ANFISs have lowest GMPP oscillations. GWOs will be unable to catch new GMPPs when they alters their position since all wolves will be looking in the prior GMPPs search zone. As a result, if the controller detects a change in PSCs, the agents of GWOs should be re-initialized to scan the search region for new GMPPs. ANFISs will follow GWOs once they have identified GMPPs until the controller detects another change in the PSCs.

If the condition stated in equation (27) is true, the controller will follow the PSCs modification. Figure 7 shows a flowchart which summarizes processes of hybrid GWO-ANFIS with PSCs modification re-initialized.

4.2. The Charge and Discharge Control. Power is transferred from and to the battery bank via the charging and discharging controller. The bidirectional converter in the standalone PV system with the battery bank illustrated in Figure 8 has four distinct control modes depending on magnitude of power produced by PV array, that is dependent on temperature and irradiance.

Mode 1. When obtained PV power is less than power needed by EVs battery, i.e. PPV < PDDh, and the charge status of SOC is greater than 40%, first control mode is used.

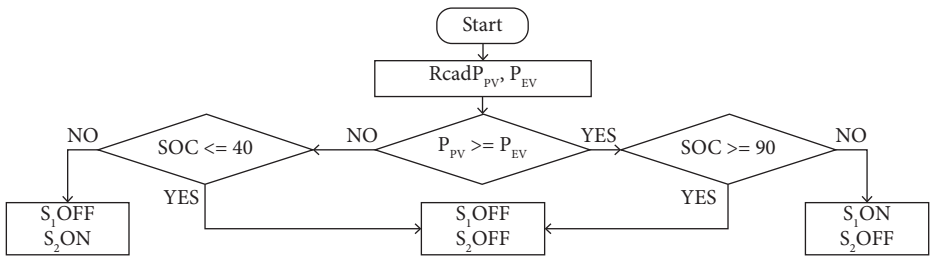

Figure 8: Four operating modes flowchart.

The bidirectional converter enters buck mode in this mode, where the controller sends a control signal to make switch 1 (S1) detached while also sending a control signal to make switch 2 (S2) connect. This mode uses storage batteries to offer additional power.

Mode 2. When obtained PV power is less than power needed by EVs battery, i.e. PPV < PDDh, and the charge status of SOC is less than 40%, the second control mode is used. In this mode, the controller sends a control signal to both switches 1 (S1) and 2 (S2), causing them to be disconnected.

Mode 3. When obtained PV power exceeds power needed by EVs battery, i.e., PPV > PDDh and the charge status of SOC is less than 90% and more than 40%, the third control mode is used. PV array not only supplies power to EVs battery under maximum power point enabled management in this mode, but it also charges the battery bank with surplus power produced by PV array. In this mode, the controller sends a control signal to switch 1 (S1) to connect and a control signal to switch 2 (S2) to disconnect, causing the bidirectional converter to enter boost mode.

Mode 4. When the generated PV power exceeds the EVs battery's power demand, i.e., PPV > PDDh, and the storage battery's charge state (SOC) is greater than 90%, the fourth control mode is used. The PV array delivers power to EVs battery under maximum power point enabled management in this mode, and charge status of storage battery is maintained at more than 90% by constant voltage charging to prevent the battery from discharging. In this mode, the controller sends a control signal to both switches 1 (S1) and 2 (S2), causing them to be disconnected. The four operational modes are depicted in Figure 8's flowchart.

5. Simulation Result

Simulating the suggested TPC Converter for performance assessment with the Sim Power-System Toolbox is done in MATLAB/Simulink setting. DC-microgrid settings provided in Table 1 were used to obtain all simulation results in MATLAB 2021.

The solar irradiation fluctuates as per the following pattern in the simulation, while all other parameters remain constant. As a consequence of GWO-ANFIS MPPTs, the DC-microgrid is at steady state at $t = 0$ s, and the four PV at 1000 wb/m^2 create the current I_{PV} of 6.8 Amps, the PV output voltage V_{PV} of 125.8 Volt, and the PV power P_{PV} of 856 watts as seen in Figure 9. There is no bypass diode conduct since all four PVs are operated in equal irradiance with just one global peak, as illustrated in Figure 10. As indicated in Figure 11, the EVs charging power P_{EV} from the DC micro grid is 700 Watts, with a nominal dc link voltage V_{EV} of 110 V and an EVs current I_{EV} of 6.36 Amps. The remaining PV power P_{ESS} of 150 Watts is stored in the ESS battery at a current I_{ESS} of −2.49 A and a voltage of 60.2 Volt, increasing the battery SOC from 40% to 60%, as illustrated in Figure 12.

Table 1: Parameters used in simulation.

Sl.no	Parameter	Value
1	PV MPP power (P_{MPP})	213.15 W
2	PV MPP voltage (V_{MPP})	29 V
3	PV MPP current (I_{MPP})	7.35 A
4	Series PV panel	4No's
5	Parallel PV panel	1No's
6	Storage system battery type	Lead-acid
7	Storage system battery nominal voltage (V_{SSV})	60 V
8	Storage system battery rated capacity	16 Ah
9	SEPIC converter inductors ($L_{\mathrm{SEPIC-1}}$&$L_{\mathrm{SEPIC-2}}$)	1.6 mH
10	SEPIC converter coupling capacitor (C_C)	10 μF
11	Buck converter inductor (L_{BUCK})	3.3 mH
12	Bidirectional converter inductor (L_{BI})	2.4 mH
13	DC link capacitor (C_{DC})	60 μF

Due to partial shade, the irradiation of Panels 3 and 4 drops to 300 wb/m^2 at $t = 0.2$ s. PV output voltage V_{PV} falls to 59.5 Volts, PV current I_{PV} reduces to 7.1 amps, and PV power P_{PV} falls to 422.5 Watts. As illustrated in Figure 10, this global power is tracked using the GWO-ANFIS MPPTs algorithm by removing the darkened panel at this instant bypass diode conduction. Even when the PV lighting varies, the DC bus voltage remains constant at 110 V thanks to the battery converter. At $t = 0$ s, the battery is charging, but as the PV output power decreases, it drains. Because the DC bus voltage remains constant at 110 V, EVs power P EVs is kept constant at 700 W, as illustrated in Figure 11. The remaining power P_{ESS} of 277.5 Watts obtained by PV is stored in ESS battery at a current I_{ESS} of 4.64 A and a voltage of 59.7 Volt, lowering the battery SOC from 40% as seen in Figure 12

The PV panel and diesel generator are started with a produced power of 422.5 watts and 790 watts, respectively, as the ESS battery discharges below 40% SOC at $t = 0.4$ sec, as illustrated in Figures 9 and 13. To keep the EVs power P_{EV} at 700 W, the DC bus voltage is kept constant, as illustrated in Figure 11. He remaining power P_{ESS} of 512.5 watts charged in the ESS battery, increasing the SOC as illustrated in the Figure 12.

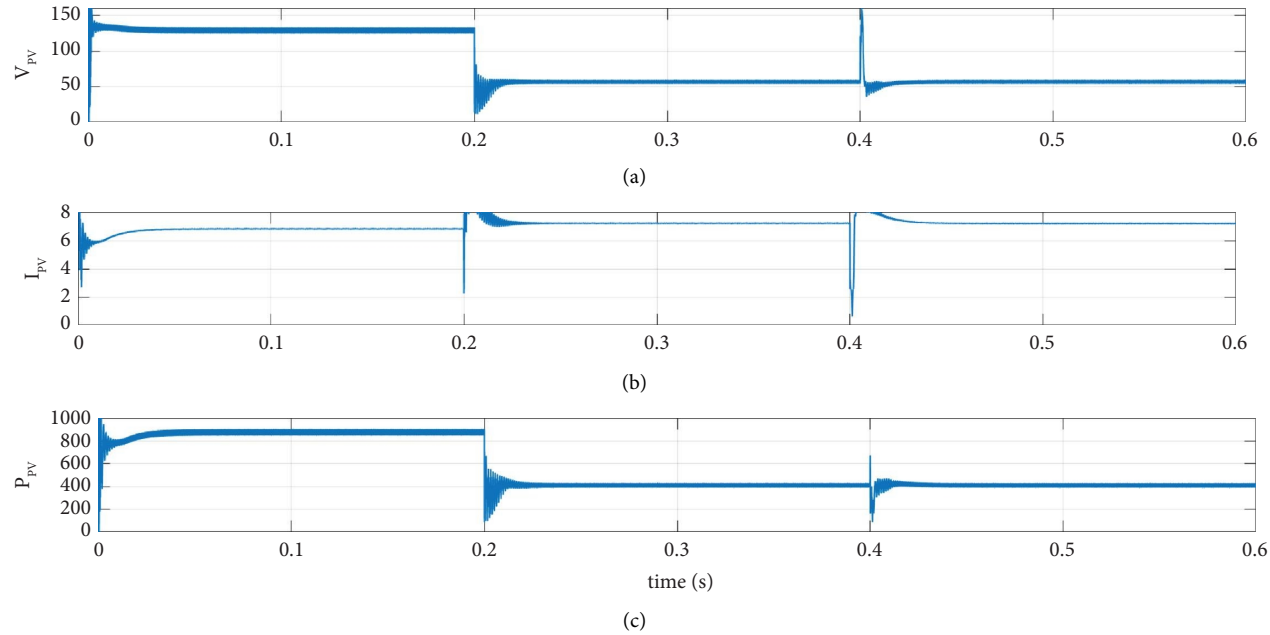

Figure 9: Simulation results (a) PV voltage (b) PV current (c) PV power.

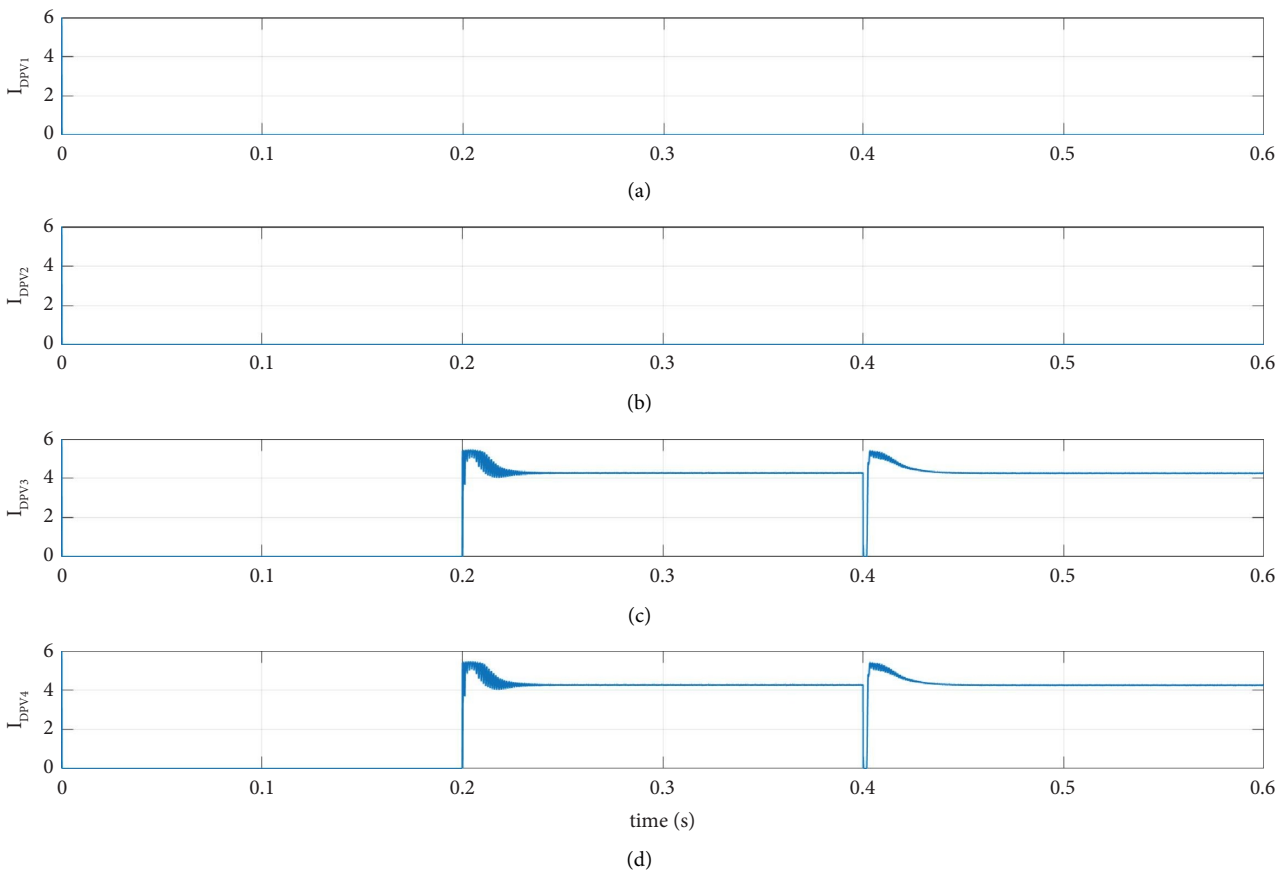

Figure 10: Simulation results (a) bypass diode PV -1 (b) bypass diode PV -2 (c) bypass diode PV -3 (d) bypass diode PV -4.

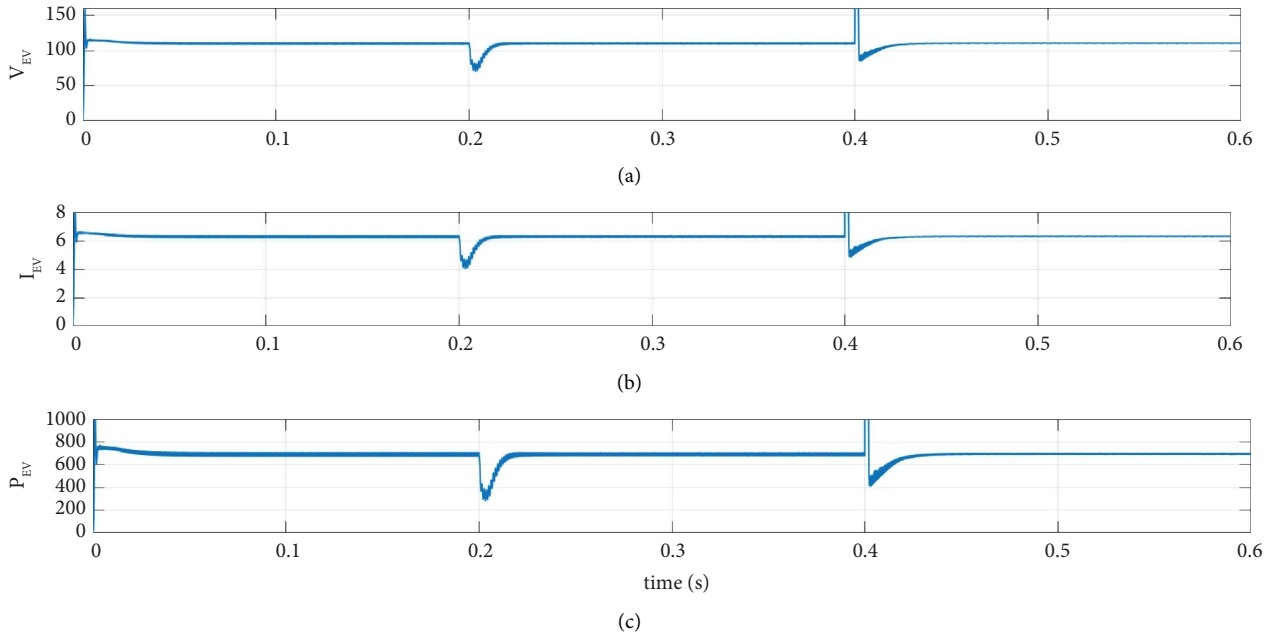

Figure 11: Simulation results (a) EVs voltage (b) EVs current (c) EVs power.

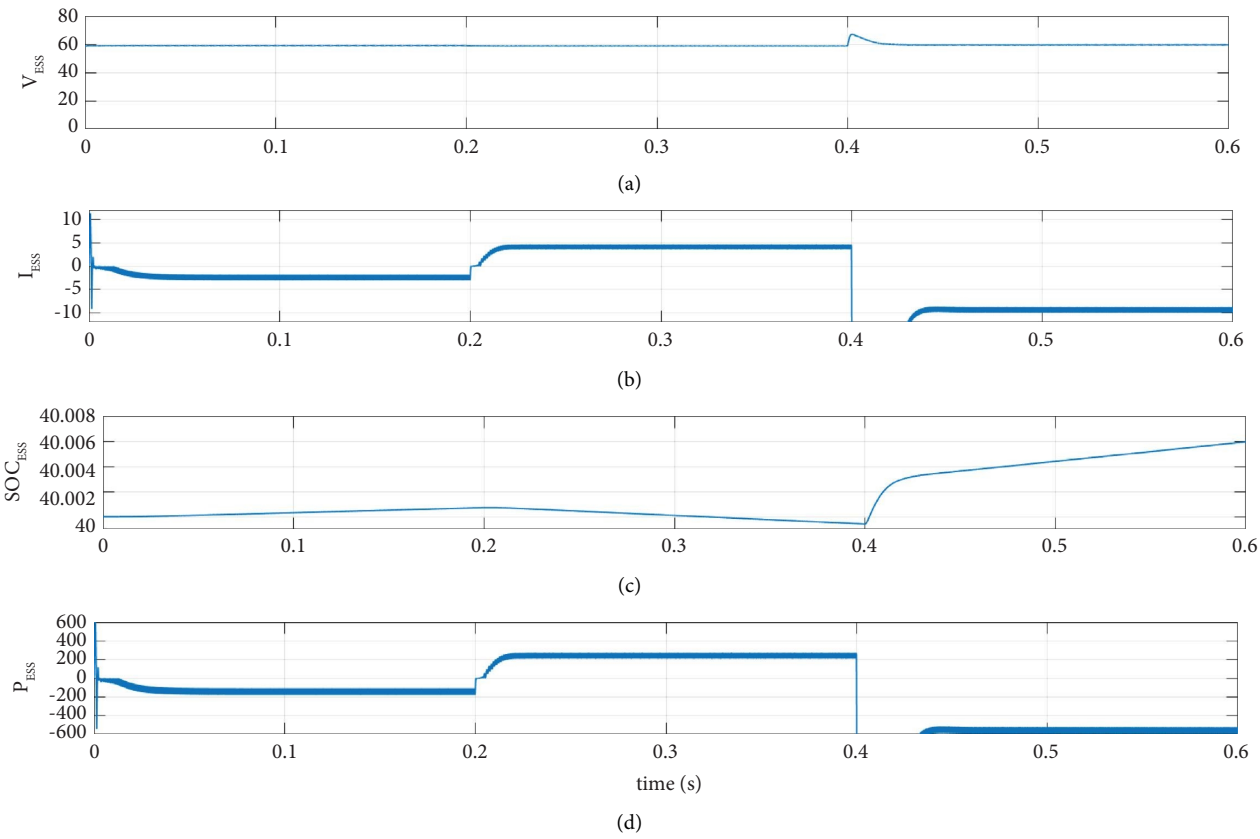

Figure 12: Simulation results (a) ESS voltage (b) ESS current (c) ESS SOC (d) ESS power.

6. Experimental Results

The proposed GWO-ANFIS tracking algorithm has been evaluated for its performance with P&O MPP tracking algorithms. The evaluation tracked maximum power from PV array system to DC using a simple boost converter. Table 2 lists hardware parameter values of 4S configuration in Proposed GWO-ANFIS MPPT.

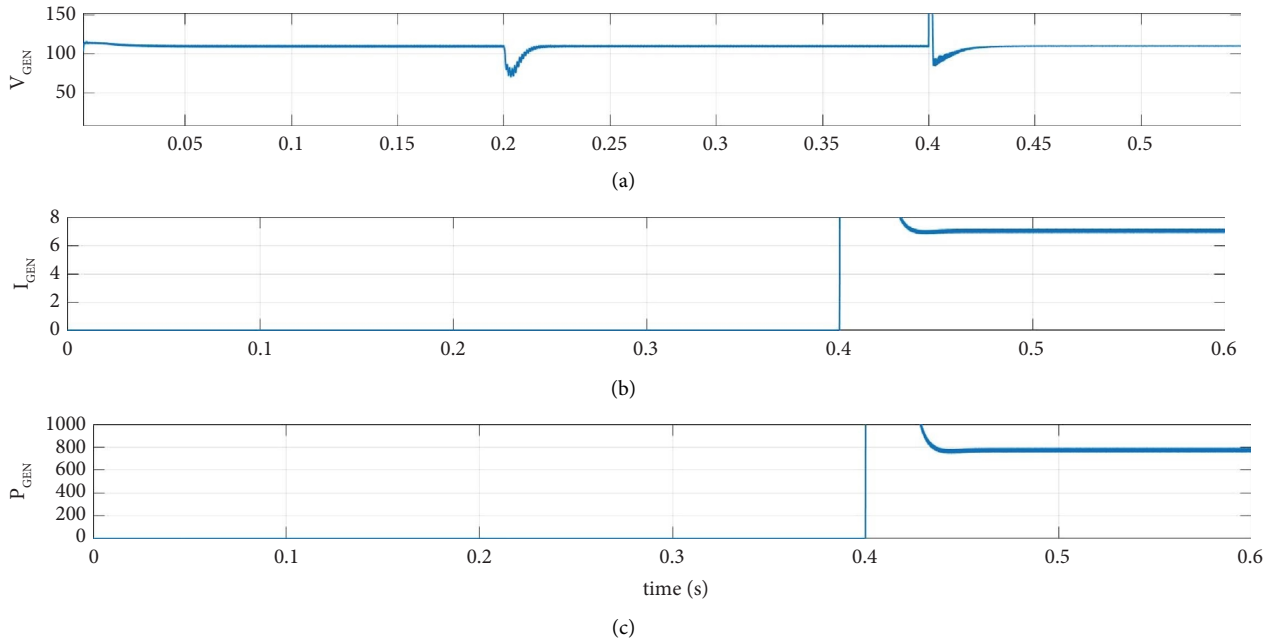

Figure 13: Simulation results (a) diesel generator voltage (b) diesel generator ESS current (c) diesel generator power.

Table 2: Hardware parameter values of 4S configuration.

Parameter		Value
Boost inductance	4S	2.36 mH
DC filter capacitor	4S	200 μF
Load resistor	4S	140 ohms
MOSFET 400 V, 10 A, N-channel		IRF740
Schottky diode 200 V, 10 A		MUR 10200
Maximum power PVC current (I_{mpp})		2.90 A
Maximum power PVC voltage (V_{mpp})		17.5 V
Maximum power PVC power (P_{mpp})		50 W
Open circuit PVC voltage (V_{oc})		21.8 V
Sort circuit PVC current (I_{sc})		3.20

(a) (b)

Figure 14: Experimental results for proposed GWO-ANFIS MPPT method for 4S configuration. (a) Pattern 1. (b) Pattern 2.

To validate the effectiveness of the proposed MPPT, experiments were carried out on real PV array for both 4S. To create partial shading, transparent sheets of different shapes were placed on PV modules.

Figures 14(a) and 14(b) shows the PV voltage, PV current and PV power of GWO-ANFIS based MPPT control at 4S configuration with two different Pattern-1 and Pattern-2 respectively. The corresponding values are denoted in Table 3.

Table 3: Performance comparison of the proposed GWO-ANFIS MPPT method for 4S configuration.

Shading pattern	GP in watts	V_{PV}	I_{PV}	P_{PV} (W)	Track efficiency (%)
Pattern 1	108.2 W/75.5 V	75.7	1.41	106.74	98.65
Pattern 2	76.33 W/35.8 V	35.1	2.13	74.76	97.94

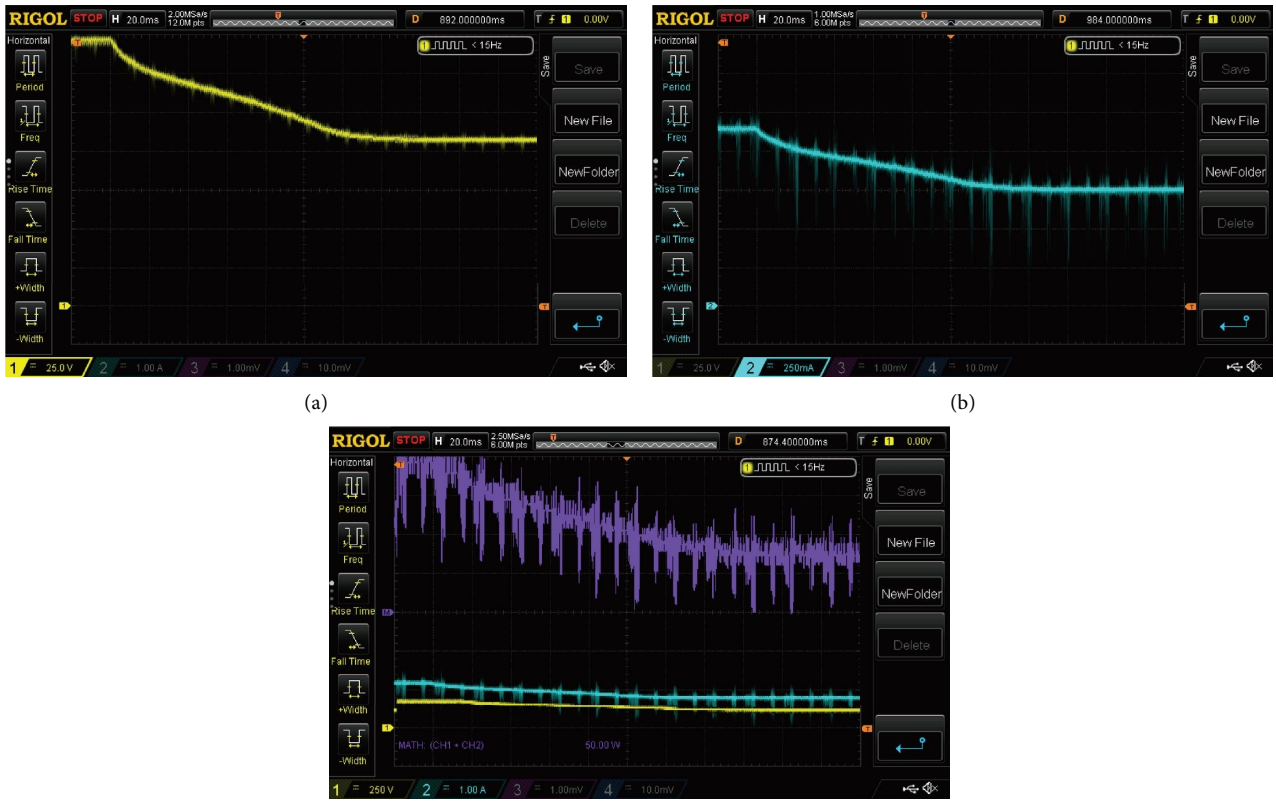

Figure 15: Experimental result of proposed GWO-ANFIS MPPT for pattern 2. (a) DC link voltage. (b) DC link current. (c) DC link power.

Figure 15. Shows the DC Voltage, DC current and DC power of Proposed GWO-ANFIS MPPT algoritham for Pattern2.

7. Conclusion

This article successfully built and simulated a charging station that use s a stand-alone PV system with an energy storage system to charge an EVs battery. The GWO-ANFIS method has been used with the MPPT controller. The P-V curve has several peaks due to partial shading; one GMPPs and many LMPPs. Heuristic approaches such as GWOs can readily capture the GMPPs before it starts hunting. The results showed that GWO-ANFIS with PSCs change re-initialization is the optimum approach for tracking the dynamic GMPPs. The combination of the ANFISs controller and the GWOs method significantly reduced output power oscillations. The charge and discharge phases of the battery energy storage were also effectively modelled and simulated employing the bidirectional converter. A bidirectional converter logic controller has also been created and simulated. The logic controller's efficiency with the bidirectional controller was demonstrated by the findings. The suggested station's design and power management are discussed and evaluated in MATLAB/Simulink using three alternative modes of operation. The experimental verification is done for PV 4S configuration using GWO-ANFIS MPPT with Boost converter which proves that the maximum power is tracked in PSC at an efficiency 98.65%.

Data Availability

Data sharing not applicable to this article as no datasets were generated or analysed during the current study. No underlying data was collected or produced in this study.

Ethical Approval

In our work, no animals or human are involved.

Conflicts of Interest

The authors declare they have no conflicts of interest.

References

[1] J. A. P. Lopes, F. J. Soares, and P. M. R. Almeida, "Integration of electric vehicles in the electric power system," *Proceedings of the IEEE*, vol. 99, no. 1, pp. 168–183, 2011.

[2] A. S. B. Humayd and K. Bhattacharya, "A novel framework for evaluating maximum PEV penetration into distribution systems," *IEEE Transactions on Smart Grid*, vol. 9, no. 4, pp. 2741–2751, Jul 2018.

[3] K. Clement-Nyns, E. Haesen, and J. Driesen, "The impact of charging plug-in hybrid electric vehicles on a residential distribution grid," *IEEE Transactions on Power Systems*, vol. 25, no. 1, pp. 371–380, 2010.

[4] K. Qian, C. Zhou, M. Allan, and Y. Yuan, "Modeling of load demand due to EV battery charging in distribution systems," *IEEE Transactions on Power Systems*, vol. 26, no. 2, pp. 802–810, 2011.

[5] J. Van Roy, N. Leemput, F. Geth, R. Salenbien, J. Buscher, and J. Driesen, "Apartment building electricity system impact of operational electric vehicle charging strategies," *IEEE Transactions on Sustainable Energy*, vol. 5, no. 1, pp. 264–272, 2014.

[6] S. Shafiee, M. Fotuhi-Firuzabad, and M. Rastegar, "Investigating the impacts of plug-in hybrid electric vehicles on power distribution systems," *IEEE Transactions on Smart Grid*, vol. 4, no. 3, pp. 1351–1360, Sep 2013.

[7] C. B. Harris and M. E. Webber, "The impact of vehicle charging loads on frequency regulation procurements in ERCOT," in *Proceedings of the ISGT 2014*, pp. 1–5, Washington, DC, USA, February, 2014.

[8] E. Sortomme, M. M. Hindi, S. D. J. MacPherson, and S. S. Venkata, "Coordinated charging of plug-in hybrid electric vehicles to minimize distribution system losses," *IEEE Transactions on Smart Grid*, vol. 2, no. 1, pp. 198–205, Mar 2011.

[9] M. Akmal, A. Jawad, and A. Al Tarabesheh, "Design and simulation solar grid-connected charger for electrical vehicles," in *Proceedings of the UKSim AMSS 20th International Conference on Modelling& Simulation*, Cambridge, UK, March 2018.

[10] G. I. Rashed, "Applicability study of battery charging stations in off-grid for rural electrification – the case of Rwanda," in *Proceedings of the International Conference on Power Generation Systems and Renewable Energy Technologies (PGSRET)*, pp. 1–6, Istanbul, Turkey, August 2019.

[11] M. Ishaq, U. H. Ibrahim, and H. Abubakar, "Design of an off grid photovoltaic system: a case study of government technical college, wudil, kano state," *International Journal of Scientific & Technology Research*, vol. 2, no. 12, pp. 172–181, December 2013.

[12] F. J. Vivas, A. De lasHeras, F. Segura, and J. M. Andújar, "A review ofenergy management strategies for renewable hybrid energy systems withhydrogen backup," *Renewable and Sustainable Energy Reviews*, vol. 82, pp. 126–155, Feb. 2018.

[13] A. Amjad, L. Wuhua, and H. Xiangning, "Simple moving voltage averageincremental conductance MPPTs technique with direct control methodundernonuniform solar irradiance conditions," *International Journal of Photoenergy*, vol. 2015, Article ID 479178, 12 pages, Jan. 2015.

[14] D. Verma, S. Nema, A. M. Shandilya, and S. K. Dash, "Maximumpower point tracking (MPPTs) techniques: recapitulation in solar photovoltaicsystems," *Renewable and Sustainable Energy Reviews*, vol. 54, pp. 1018–1034, Feb. 2016.

[15] B. Subudhi and R. Pradhan, "A comparative study on maximum powerpoint tracking techniques for photovoltaic power systems," *IEEE Transactions on Sustainable Energy*, vol. 4, no. 1, pp. 89–98, Jan. 2013.

[16] M. A. Elgendy, B. Zahawi, and D. J. Atkinson, "Assessment of perturb and observe MPPT algorithm implementation techniques for PV pumping applications," *IEEE Transactions on Sustainable Energy*, vol. 3, no. 1, pp. 21–33, Jan. 2012.

[17] M. A. Elgendy, B. Zahawi, and D. J. Atkinson, "Operating characteristics of the P&O algorithm at high perturbation frequencies for standalone PV systems," *IEEE Transactions on Energy Conversion*, vol. 30, no. 1, pp. 189–198, Jun. 2015.

[18] M. A. Elgendy, B. Zahawi, and D. J. Atkinson, "Assessment of the incrementalconductance maximum power point tracking algorithm," *IEEE Transactions on Sustainable Energy*, vol. 4, no. 1, pp. 108–117, Jan. 2013.

[19] M. A. G. de Brito, L. Galotto, L. P. Sampaio, G. d. A. e Melo, and C. A Canesin, "Evaluation of the main MPPT techniques for photovoltaic applications," *IEEE Transactions on Industrial Electronics*, vol. 60, no. 3, pp. 1156–1167, Mar. 2013.

[20] A. S. Mahdi, A. K. Mahamad, S. Saon, T. Tuwoso, H. Elmunsyah, and S. W. Mudjanarko, "Maximum power point tracking using perturb and observe, fuzzy logic and ANFIS," *SN Applied Sciences*, vol. 2, no. 1, 2020.

[21] R. Kotti and W. Shireen, "EfficientMPPT control for PV systems adaptiveto fast changing irradiation and partial shading conditions," *Solar Energy*, vol. 114, pp. 397–407, Mar. 2015.

[22] K. Ishaque, Z. Salam, M. Amjad, and S. Mekhilef, "An improved particle Swarm optimization (PSO)–Based MPPT for PV with reduced steady-state oscillation," *IEEE Transactions on Power Electronics*, vol. 27, no. 8, pp. 3627–3638, 2012.

[23] S. Mirjalili, S. M. Mirjalili, and A. Lewis, "Grey wolf optimizer," *Advances in Engineering Software*, vol. 69, pp. 46–61, 2014.

[24] L. L. Jiang, D. L. Maskell, and J. C. Patra, "A novel ant colony optimization-based maximum power point tracking for photovoltaic systems under partially shaded conditions," *Energy and Buildings*, vol. 58, pp. 227–236, 2013.

[25] K. Sundareswaran, S. Peddapati, and S. Palani, "MPPTs of PV systemsunder partial shading conditions through a colony of flashing fireflies," *IEEE Transactions on Energy Conversion*, vol. 29, no. 2, pp. 463–472, Jun. 2014.

[26] L. L. Jiang, R. Srivatsan, and D. L. Maskell, "Computational intelligence techniques for maximum power point tracking in PV systems: a review," *Renewable and Sustainable Energy Reviews*, vol. 85, pp. 14–45, 2018.

[27] F. Belhachat and C. Larbes, "A review of global maximum power point tracking techniques of photovoltaic system under partial shading conditions," *Renewable and Sustainable Energy Reviews*, vol. 92, pp. 513–553, 2018.

[28] A. A. Mohamed, H. Metwally, A. El-Sayed, and S. I. Selem, "Predictive neural network based adaptive controller for grid-connected PV systems supplying pulse-load," *Solar Energy*, vol. 193, pp. 139–147, 2019.

[29] O. P. Pahari and B. Subudhi, "Integral sliding mode-improved adaptive MPPT control scheme for suppressing grid current harmonics for PV system," *IET Renewable Power Generation*, vol. 12, no. 16, pp. 1904–1914, 2018.

[30] A. Kihal, F. Krim, A. Laib, B. Talbi, and H. Afghoul, "An improved MPPT scheme employing adaptive integral derivative sliding mode control for photovoltaic systems under fast irradiation changes," *ISA Transactions*, vol. 87, pp. 297–306, 2019.

[31] S. Pareek and T. Kaur, "Hybrid ANFIS-PID based MPPTs controller for a solar PV system with electric vehicle load IOP conference series: materials science and engineering," *IOP Conference Series: Materials Science and Engineering*, vol. 1033, no. 1, Article ID 012012, 2021.

[32] S. Padmanaban, N. Priyadarshi, M. Sagar Bhaskar, J. B. Holm-Nielsen, V. K. Ramachandaramurthy, and E. Hossain, "A hybrid ANFIS-ABC based MPPTs controller for PV system with anti-islanding grid protection: experimental realization," *IEEE Access*, vol. 7, Article ID 103377103389, 2019.

[33] R. Kumar, S. Khandelwal, P. Upadhyay, and S. Pulipaka, "Global maximum power point tracking using variable sampling time and pv curve region shifting technique along with incremental conductance for partially shaded photovoltaic systems," *Solar Energy*, vol. 189, pp. 151–178, 2019.

[34] K. Muralidhar and S. Susovon, "An adaptive voltage sensor based MPPTs for photovoltaic systems with SEPIC converter including steady state and drift analysis," *IEEE Transactions on Industrial Electronics*, vol. 62, no. 12, pp. 992–1000, Dec 2015.

[35] S. Naeim, "Design of a DC/DC buck converter for ultra-low power applications in 65nm CMOS Process," Master's thesis, Linköping University, Linköping, Sweden, 2012.

[36] C. Kuei-Hsiang, T. Ming-Chang, H. Chun-Hao, L. Yang-Guang, and H. Liang-Chiao, "Design and implementation of a bidirectional DC-DC converter for stand-alone photovoltaic systems," *International Journal of Computers, Communications & Control*, vol. 2, no. 3, 2013.

[37] S. K. Cherukuri and S. R. Rayapudi, "Enhanced grey wolf optimizer basedMPPT algorithm of PV system under partial shaded condition," *International Journal of Renewable Energy Development*, vol. 6, no. 3, 2017.

[38] F. Liu, P. Yadav, A. M. Baschnagel, and A. B. McMillan, "MR-based treatment planning in radiation therapy using a deep learning approach," *Journal of Applied Clinical Medical Physics*, vol. 20, no. 3, pp. 105–114, 2019.

[39] S. Remya, J. E. Paul, and D. B. Nair, "ANFIS based SEPIC converter for maximum power point tracking of photovoltaic modules," *International Journal of Engineering Trends and Technology*, vol. 30, no. 4, pp. 170–175, 2015.

[40] M. S. Kumar, P. S. Manoharan, and R. Ramachandran, "Modelling and simulation of ANFIS-based MPPT for PV system with modified SEPIC converter," *International Journal of Business Intelligence and Data Mining*, vol. 15, no. 3, pp. 255–272, 2019.